Dynamic magnetic resonance imaging in assessment of tumour blood flow and oxygenation

M. Muruganandham and V. Jain*

Department of Biocybernetics, Institute of Nuclear Medicine and Allied Sciences, Delhi 110 054, India
*Present address: Dr Ambedkar Center for Biomedical Research, University of Delhi, Delhi 110 007, India

Tumour blood flow and oxygenation are among the important determinants of various non-surgical forms of cancer treatments. To improve the treatment efficacy, several agents that modify blood flow in tumours are currently under intensive investigation. Thus a noninvasive approach to study the effects of these agents on tumour blood flow and oxygenation would be of great use. Recent advances in magnetic resonance imaging (MRI) methodology make it possible to monitor dynamically the changes in tissue blood flow and oxygenation with a better spatial and temporal resolution. In this context, the applications of dynamic Gd-DTPA and BOLD contrast enhanced MRI to monitor the changes in tumour blood flow and oxygenation are reviewed in the present article. The usefulness of such measurements in tumour radiotherapy is illustrated by studies on the effects induced by diltiazem, a calcium channel blocker, on a murine tumour model.

IT is now increasingly realized that the responses of solid tumours to non-surgical treatment modalities are profoundly influenced by the pattern of blood flow and supply of nutrients such as glucose and oxygen. These physiologic parameters, which affect the microenvironment and the metabolic activity, are different in tumours than those in normal tissues from which they arise. Therefore, modulation of tumour physiology and metabolism for anti-cancer therapy has received increasing attention in recent times along with the approaches based on cellular and molecular differences between normal and cancer cells[1–3].

Tumour vascular network and blood flow

The underlying differences in the physiology of normal and tumour tissues stem from the peculiar tumour vascular network which is composed of two types of blood vessels: (i) the pre-existing vessels in normal tissues into which tumour has invaded and (ii) newly induced tumour micro-vessels arising from neovascularization. The pre-existing host vasculature provides the structures from which neovasculature arises[4–6]. With tumour growth, however, the host vessels per unit mass of tumour do not increase in number, thus leading to a reduction of available exchange area for oxygen, nutrients, growth factors and waste products[7]. The host vessels incorporated in the tumour mass also get disintegrated, obstructed, or compressed during the growth of tumour. Newly formed micro-vessels of some of the highly differentiated tumours have a matured architecture, whereas rapidly growing tumours have severe structural abnormalities in their micro-vessels[4]. Even though morphological appearance of the tumour vascular bed does not directly correlate with microcirculation/nutritive blood flow, high vascular density facilitates adequate nutritive blood flow, which in turn will affect treatment response[8]. Also the O_2 pressure profile within the capillaries and the inter-capillary distance in tumours profoundly influence the tumour oxygenation and thereby affect therapeutic response[9].

Considerable spatial and temporal heterogeneity in the microcirculation exists among individual vessels, in different microareas within a given tumour as well as in tumours of similar origin at different sizes, having the same grading and staging, and between tumours of different histologies[4,8]. In general, most tumours contain regions of high perfusion (i.e. the supply of nutrients, oxygen and removal of waste products to/from tissues through capillaries), which are rapidly growing and which infiltrate the normal surroundings, and also areas with compromised and sluggish perfusion often associated with the development of necrosis (cell death and degradation). Among the tumour vessels, the host vessels are relatively more responsive to physiological/pharmacological stimuli, whereas the newly recruited micro-vessels, as a result of tissue acidosis and hypoxia/anoxia, are maximally dilated and less reactive. Therefore, the microcirculatory regulation depends on the proportions of host vessels that are present in the tumour. The ratio of the host vessels to newly formed vessels varies from one location to another, from time to time and from one tumour to another. These characteristics of tumour vasculature lead to heterogeneous blood flow within the tumour.

The heterogeneity in blood flow within a tumour may result in anisotropic distribution of tumour tissue oxygenation, nutrient supply, tissue pH, and bioenergetic status, factors which are important determinants of tumour response to various therapies[8]. In chemotherapy and immunotherapy, the status of blood flow within the tumour determines the delivery of drugs/antibodies to tumour cells. Similarly in radiation therapy, hypoxic tumour cells (i.e. cells having partial oxygen tension ≤ 10 mm Hg) are rela-

tively resistant to radiation as compared to the normoxic cells. Thus, the responses of tumours to these treatments are mainly determined by the status of tumour blood supply and oxygenation. Several agents that modify blood flow in tumours are currently under intensive investigation with an aim to improve the treatment efficiency[10–13]. Effects of these agents on tumour blood flow/oxygenation are investigated, at present, using a variety of methods, viz. radioactive tracers[14], fluorescent perfusion markers[15], microelectrodes[16] and Laser–Doppler velocimetry[17]. These methods are, however, limited to observations only from small portions of the tumour and repeated measurements on the same tumour are often difficult. Several MR methods employing different techniques such as quantitative D_2O spectroscopy[18,19], ^{19}F spectroscopy with perfluorocarbons as tracers[20,21], ^1H spectroscopic imaging[22], endogenous[23] and exogenous contrast enhanced MRI[24] are also being developed. In general, the MR methods have the advantage of being not only noninvasive but also permitting easy and repetitive measurements with better spatial and temporal resolution to study tumour physiology and to monitor the tumour response to treatment. In the following, methods based on contrast enhanced MRI techniques are described in some detail since these methods can be easily implemented with most of the commercial, presently available systems.

Dynamic contrast enhanced MR techniques

With the advent of ultrafast, high-spatial and temporal resolution imaging and the understanding of exogenous/endogenous contrast materials, it is now possible to observe functional properties in addition to structural properties of regions of interest that hitherto remained obscure. Generally, the signal intensity in MR images depends on the spin density (the local hydrogen concentration) as well as longitudinal (T_1) and transverse (T_2) relaxation times of different tissues, and the movement of water protons (blood flow related as well as Brownian motion). The image contrast (i.e. differences in the MR signals) can be made more specific to each one of these tissue-dependent relaxation characteristics by using selective pulse sequences – that is, the selection of the timing, order, polarity, and repetition frequency of the RF pulses and applied magnetic field gradients. In a typical imaging protocol, using spin-echo pulse sequence, the signal intensity, I, for a specific area in the image can be empirically stated as:

$$I \propto M_0 (1 - e^{-TR/T_1}) e^{-TE/T_2} \propto M_0 (1 - e^{-TR.R_1}) e^{-TE.R_2}, \quad (1)$$

where M_0 is the equilibrium magnetization of tissue water protons and depends on the applied external magnetic field, TR is the repetition time (i.e. the time between two successive RF pulses), TE is the echo time (i.e. the time from initial RF pulse to the peak of the emitted MR signal), R_1 ($= 1/T_1$) and R_2 ($= 1/T_2$) are the longitudinal and transverse relaxation rates respectively. The values of the machine dependent parameters TR and TE can be selected appropriately to get the T_1 or T_2 weighted images of the tissues. Thus, in a gradient-echo pulse sequence which exploits the differences in tissue susceptibilities, the signal intensity can be expressed as:

$$I \propto M_0 e^{-TE/T_2^*} \propto M_0 e^{-TE.R_2^*}, \quad (2)$$

where the observed (or effective) relaxation rate $R_2^* = R_2 + R_2'$ and R_2' is the contribution from (macroscopic and microscopic) local magnetic field inhomogeneities (known as the susceptibility effect).

The endo- and exogenous contrast agents used to probe physiologic characteristics of the tissues affect tissue water R_1 and R_2 either through direct T_1 relaxivity and/or through indirect susceptibility effects and these effects can be expressed[25–30] as

$$R_{1c} = R_{10} + r_1 [C], \quad (3)$$

and

$$R_{2c} = R_{20} + r_2 [C], \quad (4)$$

where R_{1c}, R_{2c} are relaxation rates in the presence of contrast agent and R_{10}, R_{20} are the precontrast relaxation rates; r_1, r_2 are the longitudinal and transverse relaxivities, values that characterize the efficiency with which an agent enhances tissue water proton relaxation[31]. Thus the dynamic MR measurements of contrast agent-induced effects on tissue T_1 and T_2 relaxation processes would reflect as changes in image contrast, which in turn, provide information on tissue physiology.

The imaging protocol would include either T_1 (relaxivity)-weighted[32,33] or T_2^* (susceptibility)-weighted[34,35] sequences. Techniques for T_2^*-weighted imaging for dynamic exogenous contrast include gradient-echo[36] and echo-planar imaging (EPI)[37]. T_2^*-weighted sequences can be readily implemented in the evaluation of brain parenchyma because the intracranial structures are relatively homogeneous. It is more difficult to implement T_2^*-weighted sequences in extracranial tissues, because of the field inhomogeneity effects. Furthermore, for a reliable assessment of concentration–time curves in tissue, T_2^* imaging requires the contrast material to remain strictly intravascular. Tumour and non-tumour tissues outside the brain do not meet this prerequisite. Under these conditions, T_1-weighted imaging methods such as conventional spin-echo or gradient-echo technique are applied. The relative changes in signal intensity provide only a qualitative information on the changes in tissue microcirculation. The quantitative information on various physiologic parameters involved in

microcirculatory changes can be derived from the T_1 data obtained during dynamic T_1 measurements and by using appropriate tracer-kinetic models[24,38].

Contrast enhancement through exogenous paramagnetic agents

When contrast agents bearing large magnetic moments are found in the vicinity of tissue protons, they can stimulate nuclear relaxation and thereby decrease both T_1 and T_2 relaxation times. Since paramagnetic ion-chelate complexes increase magnetic field inhomogeneities and also have tumbling rates that approximate Larmor frequency, they produce both T_2 and T_1 shortening[39]. Shortening of T_1 is the result of dipole–dipole interactions, which occur when the frequency of time-varying magnetic fields produced by contrast agents (as a result of molecular rotation and tumbling) is similar to resonance (Larmor) frequency of protons. Increases in local magnetic field inhomogeneities enhance dephasing of non-stationary protons, resulting in decreased T_2 or T_2^*.

Various formulations of the paramagnetic materials Gd, Dy, Mn, Fe are currently being developed. To minimize their inherent toxicity, these metals are chelated with low molecular weight ligands like diethylene-triaminepenta-acetic acid (DTPA), DTPA-bismethylamide (DTPA-BMA), and tetraazacyclododecane tetra-acetic acid meglumine (DOTA). The Gd-induced dipole–dipole interactions lead to shortening of T_1, which results in contrast enhancement on T_1-weighted images. The Gd-complexes also induce susceptibility effects, as a result of the magnetic field gradient between the blood vessels (containing the contrast agent) and the surrounding tissue, that lead to shortening of T_2 or T_2^*. These susceptibility-based effects are considerably weaker than the dipole–dipole relaxivity. Dysprosium (Dy) which possesses chemical properties similar to Gd, exhibits predominant R_2 susceptibility effect (1.8 times that of Gd) and relatively less T_1 relaxivity (1/40 of Gd) but it is more toxic than gadolinium[40].

The chelating agents of Gd are well suited for studies related to hemodynamic perturbation[41], are commercially available and therefore are generally used in clinical studies. Even though these low molecular weight complexes leak through the vascular endothelium of tumours, their contrast kinetics pattern provide information on tumour blood flow[24]. Following a contrast agent injection, tracer kinetic analysis of contrast concentration–time data can yield tissue microcirculatory information. To measure the tissue microcirculatory parameters by MR, initially, the changes in signal intensity vs time must be converted into [contrast agent concentration]$_{tissue}$ vs time curves. In a simple case, the quantitative assessment assumes a linear relation between relaxation rate R_1 and contrast agent concentration, C:

$$\Delta R_1 = R_{1C} - R_{10} = r_1 [C]. \quad (5)$$

R_{10}, R_{1C} are the blood or tissue relaxation rates measured before and after application of the contrast agent such as Gd-DTPA; and r_1 denotes the longitudinal relaxivity of Gd-DTPA.

In dynamic Gd-DTPA studies, the nature of the time intensity curve observed during first pass of the contrast material includes an early incremental phase followed by a plateau phase (Figure 1). The degree of enhancement (i.e. plateau phase, rSI) may reflect blood flow, extraction factors, and/or equilibrium distribution of the contrast agent between the tissue and blood pool. The signal intensity observed early during the first pass (i.e. the slope) represents predominantly the concentration of the contrast agent in intravascular space, whereas the peak of the time intensity curve reflects the concentration of the contrast agent both in intravascular and extravascular interstitial space[24]. The observed rate of increase in the signal intensity (i.e. value of the slope, M) is influenced by many factors such as vessel density, perfusion of the vessels, vascular resistance, vessel wall permeability, composition of the extravascular space and the venous out flow[24].

The complex pharmacokinetics of the contrast agents and their resultant effects on the observed MR signal intensity makes the interpretation of the results rather

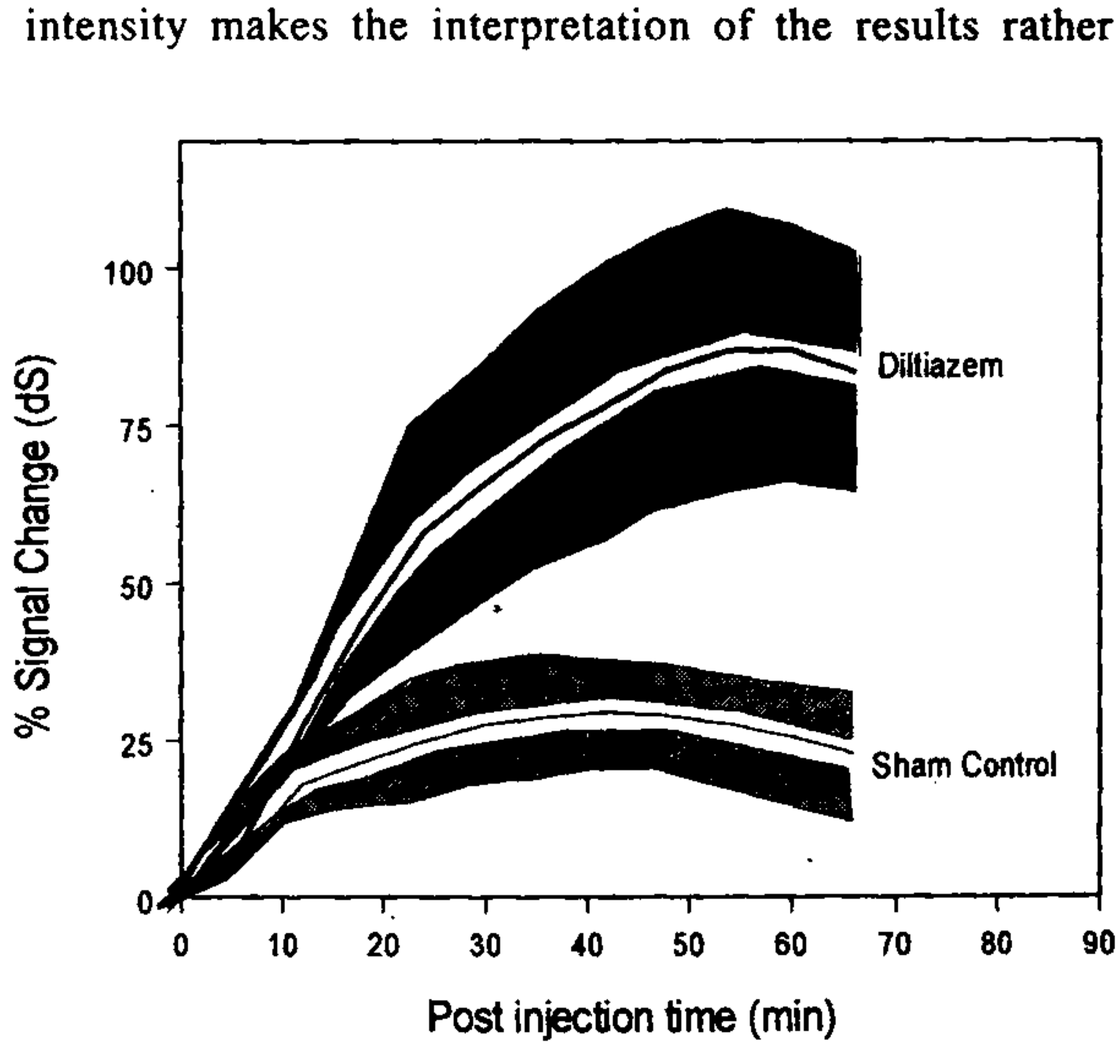

Figure 1. T_1-weighted MR gadodiamide contrast-enhancement kinetics in Ehrlich ascites tumours (EAT) in mice. Diltiazem (27.5 mg/kg) or saline mixed with contrast agent (0.2 mmol/kg) was administered as intraperitoneal single bolus injections. The shadow regions of the mean curve represent the range of data obtained from five different animals. Clear elevations in the contrast enhancement kinetics reflect the diltiazem-induced increase in tumour blood flow. The calculated slope (M) of the early incremental phase is 3.26 ± 0.61 and 1.57 ± 0.98 in diltiazem-treated and control groups respectively. The degree of enhancement (rSI), derived from the plateau phase, are $83.3 \pm 18.6\%$ and $29.3 \pm 6.8\%$ in diltiazem-treated and control groups respectively.

difficult. However, the potential usefulness of this approach in determining therapeutically significant information on tumour microcirculation[35,42] and in monitoring the effects of blood flow modifiers has been reported in various types of tumours in human as well as in animal models[33,36,43–45]. In tumour therapy, the status of tumour blood flow/oxygenation or drug concentration in the interstitial space may contribute to the effective killing of the tumour cells by irradiation or chemotherapy. In a recent study, a correlation between the increase in relative signal intensity (rSI) (representing the presence of contrast agent in the interstitial space) and the effectiveness of radiation therapy in cervical cancers has been demonstrated[35]. The increase in rSI during the early phase of radiation therapy as compared to the pre-therapy levels has been suggested to be an indicator of tumour re-oxygenation (as a consequence of improved tumour blood flow) which in turn was shown to correlate with the improved therapeutic outcome.

Enhancement of tumour blood flow by diltiazem

We have used dynamic Gd-DTPA-BMA (gadodiamide) contrast enhanced MR imaging to investigate the changes in tumour blood flow upon a pharmacological challenge[46]. The nonionic gadodiamide contrast agent, which is in routine clinical use, was selected because of its low osmolality and viscosity (thus minimizing the effects on blood rheology). The effects of a Ca^{2+} channel blocker, diltiazem, on tumour blood flow were investigated in a murine Ehrlich ascites tumour (EAT) model. T_1-weighted gadodiamide contrast enhanced MRI using RARE (*Rapid Acquisition with Relaxation Enhancement*) pulse sequence[47] was performed on a 4.7 T MRI/MRS system (Bruker Biospec) with the following parameters: TR = 150 ms, TE = 14 ms, 2 mm slice (at the tumour center), 6 cm field of view, 256 phase encoding steps, acquisition time = 5 min 41 s. Initially three pre-contrast images were obtained and after intraperitoneal injection of gadodiamide contrast mixed with diltiazem/normal saline, 11 contrast enhanced images were obtained continuously for 1 h and 6 min. FIDs of pre- and post-contrast images were processed together using an in-house algorithm. From these processed images, the region encompassing the whole tumour was selected as the region of interest (ROI). The histogram quantification of ROI was carried out. The relative signal intensity changes (ΔS) were calculated from the mean values of the histograms as follows: $\Delta S = (S_{\text{post-contrast}} - S_{\text{pre-contrast}})/S_{\text{pre-contrast}}$. The kinetic parameter, rate of enhancement (M) was calculated from the slope of the incremental phase and the degree of enhancement (rSI) was derived from the plateau phase values.

The contrast-enhancement kinetics in the tumour region is shown in Figure 1. The shadow regions of the mean curve represent the range of data obtained from five different animals. The degree (rSI) and the rate (M) of average increase in signal enhancement are considerably higher in the diltiazem-treated group as compared to the control, $83.3 \pm 18.6\%$ vs $29.3 \pm 6.8\%$ and 3.26 ± 0.61 vs 1.57 ± 0.98, respectively. Since the initial incremental phase of the kinetics reflects the presence of contrast agent inside the blood vasculature, the observed two-fold increase in M in tumours treated with diltiazem as compared to the controls reveal, indirectly, diltiazem-induced increase in tumour blood flow. Similarly the three-fold increase in the rSI values observed in diltiazem treated groups indicate the improved perfusion (diffusion of blood from the blood capillaries to the adjoining tissue space) status of the tumours. The large differences in the observed rSI values between tumours of individual mice demonstrate the inter-tumoural heterogeneity.

Contrast enhancement through endogenous paramagnetic agents

Blood oxygenation level dependent (BOLD)-MRI

The endogenous paramagnetic materials having different susceptibilities are also being studied and can be used to probe the physiological status of tissues. In a typical 70 kg human body, paramagnetic materials include iron (3–5 g), copper (70–120 mg), manganese (12 mg), nickel (10 mg), chromium (2 mg), cobalt (0.3 mg), vanadium (2 mg), molybdenum (13 mg), and tungsten (trace)[48]. Iron is approximately 30 times more abundant than all the other transition elements in a typical human body. Much of the iron is contained in the red blood cells. Thus the paramagnetic nature of iron in the blood can be exploited to unravel the physiologic aspects of the tissue *in vivo*.

The emphasis in BOLD-MRI is on the local susceptibility changes in the blood vessels based on the oxygenation-sensitive paramagnetic characteristics of blood[49,50]. In blood, deoxyhemoglobin (dHb) contains paramagnetic iron, while oxyhemoglobin (HbO_2) contains diamagnetic oxygen-bound iron. The effects of oxygenation changes in whole blood on MR signal intensity have been generally established[51–56] and the relationship between blood susceptibility and blood oxygenation has been characterized[56]. The susceptibility of completely oxygenated and completely deoxygenated red blood cells has been reported to be $-0.26 \pm 0.07 \times 10^{-7}$ and $0.157 \pm 0.07 \times 10^{-6}$ (cgs units) respectively resulting in an overall difference $\Delta\chi$ of 0.18×10^{-6} (cgs units)[56]. The paramagnetic property of blood produces bulk susceptibility difference between a blood vessel and the surrounding tissue producing resonance frequency shifts (about 1.5 ppm) in extra-vessel

molecules[57]. In the vicinity of capillaries and venules, local magnetic field distortions are generated by the presence of paramagnetic dHb in the blood. These local fields cause intravoxel phase dispersion in water protons, and the resultant image signal becomes weaker than that without phase dispersion. This effect is pronounced in gradient-echo images where the intravoxel phase dispersion directly contributes to increase in the apparent or effective transverse relaxation rate R_2^*, which depends on the level of venous blood oxygenation. Since many water molecules are affected by the changes in hemoglobin, a form of signal amplification occurs, thus the water proton BOLD-MR images can depict, at high resolution, the induced changes in tissue hemodynamics. The realization that the MR signals can be made highly sensitive to slight changes in blood oxygenation by employing susceptibility sensitive MR sequences[58] led to the use of MRI in probing tissue blood flow/oxygenation under various conditions.

At present BOLD-MRI is being extensively used to map brain functions by detecting the task-induced changes in cerebral physiology[59–62]. The utility of BOLD-MRI has also been reported in studies of heart and tumour physiology[63,64]. Karczmar *et al.* reported the effects of hyperoxia (100% O_2 breathing) on T_2^*-weighted imaging of rat tumours[64]. This hyperoxia-induced increase (30% and 50%) in tumour image intensity has been ascribed to a decrease in blood deoxyhemoglobin (an increase in T_2^*). Subsequently, the use of BOLD-contrast to probe the oxygen (100%), carbogen (5% CO_2 + 95% O_2 breathing) induced changes in tumour blood flow/oxygenation were demonstrated in various animal tumour models[65–70]. Recently, the BOLD-MR imaging has been extended to clinics to investigate the effects of carbogen breathing on human tumour[71]. These studies clearly demonstrated the prognostic as well as the diagnostic potential of the technique.

Enhancement in tumour oxygenation induced by diltiazem: BOLD-MRI studies

BOLD-MRI has also been used to investigate the effects of pharmacological agents such as hypotensive agent calcitonin gene-related peptide (CGRP) and nitric oxide donor (SIN-1) on tumour physiology[72,73]. We have studied the effects of the vasomodulator, diltiazem, on the oxygenation status of murine tumours[74]. BOLD-MR images of the murine EAT were acquired continuously before and after administration of diltiazem (27.5 mg/kg b.wt.) using a gradient-echo fast imaging sequence[75] at 4.7 T. The imaging parameters were: TR = 35 ms, TE = 9.1 ms, and the flip angle $\theta \cong 20^0$. A 2 mm slice through the tumour center was chosen, and 16 averages of 256 phase encoding steps over a 6 cm field of view were used. The duration of each image acquisition was 2.5 min. The region of interest encompassing only the tumour was selected and analysed using UXNMR image processing software. The difference (post – pre diltiazem) images displayed in Figure 2 clearly depict the heterogeneic nature of the tumour. The tumour image intensity pattern is observed to change as a function of time after the administration of diltiazem. The image hyper-intensity is seen to increase up to $25 \pm 14\%$ at 30 min following diltiazem administration. The observed variation in image intensity could be mainly due to diltiazem-induced increase in the tumour oxygenation. The impaired microcirculation in tumours may present higher levels of dHb (as discussed earlier) that would result in hypo-intense images (i.e. the baseline images acquired before diltiazem administration). The enhancement in tumour blood flow induced by diltiazem, as demonstrated by Gd-DTPA studies (Figure 1), is expected to decrease the deoxyhemoglobin to oxyhemoglobin ratio (dHb/HbO_2) resulting in hyper-intense images.

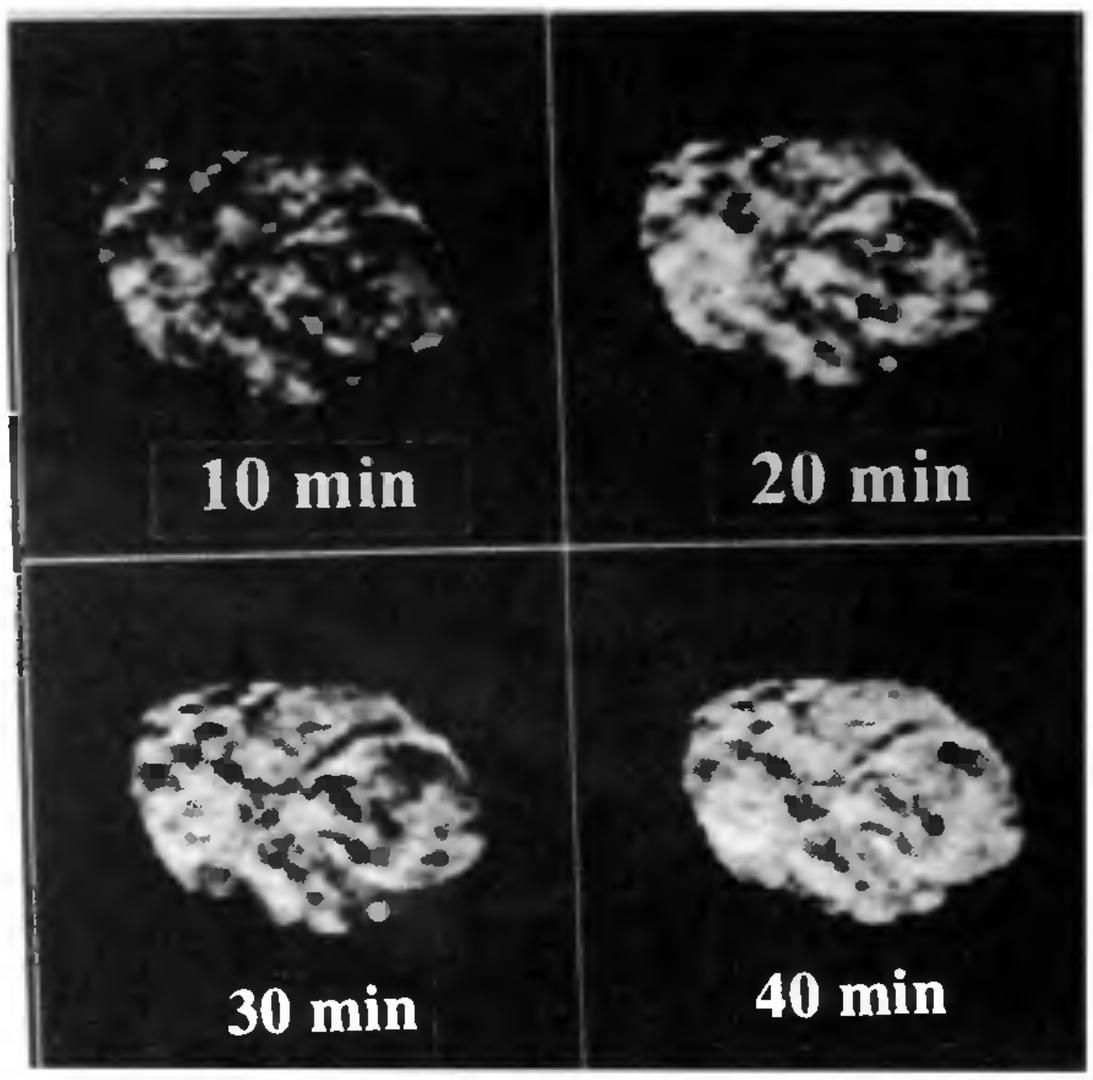

Figure 2. Blood oxygen level dependent (BOLD)-MR images of mice EAT depicting the blood flow modifying agent, diltiazem-induced increase in oxygenation. Image acquisition was carried out at 4.7 T using a susceptibility-weighted, gradient-echo fast imaging sequence (GEFI). The intensity patterns reveal the vascular status and heterogeneic nature of tumour oxygenation on a macroscopic scale. The hyper-intense regions depict the highly vascularized portions of the tumour, whereas the hypo-intense/dark regions indicate the hypoxic/anoxic/avascular nature of the tumour.

The factors other than increased tumour blood flow, like tumour cell oxygen extraction rate (OER) i.e. the respiratory rate of the tumour cells, can also influence the tumour (dHb/HbO_2) levels. Recently, Zenke *et al.*

have demonstrated the predominant effect of diltiazem on tumour blood flow in C6-glioma rat tumour model using hydrogen clearance method and electron microcytochemical studies[16]. Therefore, assuming that diltiazem does not influence tumour cell oxygen consumption and thus neglecting the contribution from OER to BOLD signal, the observed increase in the BOLD-MR image intensity could be ascribed mainly to the diltiazem induced changes in tumour oxygenation due to enhanced tumour blood flow.

Reduction of heterogeneity in tumour oxygenation and improvement in efficacy of radiotherapy by diltiazem

The BOLD-MR image intensity patterns indirectly provide insight into the structural and functional heterogeneity of tumour vasculature. In gradient-echo based BOLD measurements, the effect of intra-voxel phase dispersion of water proton spins, due to the presence of dHb-containing blood vessels, could extend up to a distance 2 times the vessel diameter[58]. Therefore in our study, the observed BOLD-MR image intensity pattern is actually the macroscopic revelation of the microvascular status. The heterogeneous nature of the tumour oxygenation is well reflected in the BOLD-MR image intensity patterns (Figure 2). The hypointense regions could represent the anoxic/hypoxic portion of the tumour. Figure 3 shows the variations in the average image intensity (calculated from histograms) of tumours as a function of time in both diltiazem-treated and sham control groups. The shadow regions of the curve represent the spread of the intensity values around the mean of five different experiments. Considerable differences observed in these intensity patterns among tumours in different mice revealed the inter-individual heterogeneity. This may be due to the presence of heterogeneous vascular density, difference in the extent of hypoxia and/or the extent of functional abnormality of the vasculature among the individual tumours. Also the large differences seen in the degree of signal enhancement (rSI) from Gd-DTPA contrast kinetics support these findings (Figure 1). The heterogeneity observed in blood flow/oxygenation could be responsible for the observed heterogeneic responses of the tumours to radiation[8]. This is also suggested by the observed diltiazem-induced enhanced radiation responses of tumours (treated with 10 Gy, single fraction of ^{60}Co-γ radiation) (Figure 4). Administration of diltiazem 30 minutes prior to radiation reduced the tumour hypoxic regions and the heterogeneity in the oxygenation status leading to improvement in therapeutic efficacy of tumour radiotherapy[76].

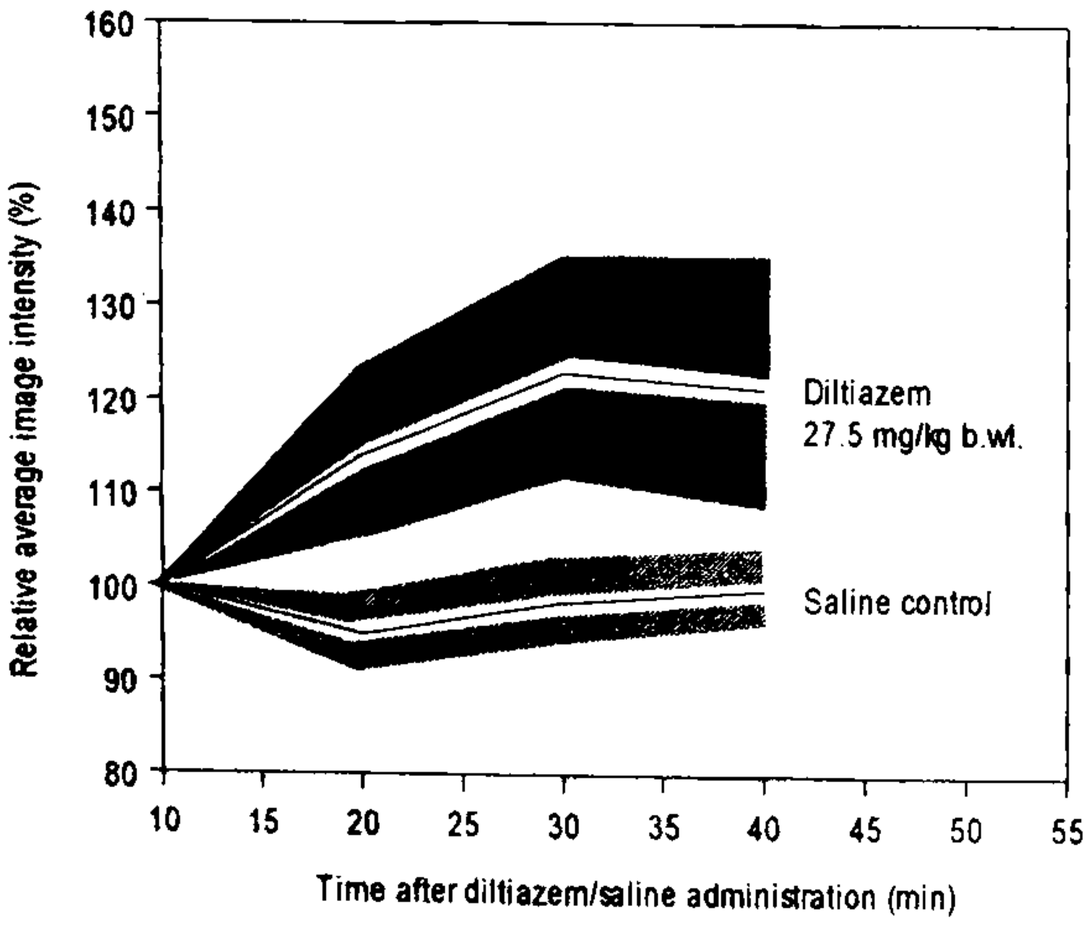

Figure 3. The average BOLD-MR image intensity (calculated from histograms) as a function of time. Shadow regions of the mean curve represent the range of data obtained from five different animals. The diltiazem-treated group shows systematic changes in tumour image intensities with maximal increase 30 min after diltiazem administration.

Quantification of observed BOLD-MRI changes in tumour oxygenation

Although measurements of the induced signal intensity changes are relatively simple and reproducible, a quantitative analysis of the observed BOLD signal changes in relation to the underlying physiologic events remain yet to be completely established. The biophysical models formulated to describe BOLD-contrast concern cerebral physiology[27–29,77–81] because of the extensive use of BOLD-MRI in cognitive neuroscience to map the brain functions. However, the same models can be applied to all perfused tissues[82]. The ultimate goal of all these models is a complete understanding of the variables that contribute to the signal changes such that changes in the blood flow, volume, and oxygenation can be accurately quantified. Recently van Zjil *et al.* have presented (in a spin-echo based BOLD-MRI) a quantitative description of the relationship between the MRI relaxation rate R_2 and basic physiological parameters of blood flow, blood volume, hematocrit and oxygen metabolic rate[82]. By using these relations and by measuring the hypoxic hypoxia-induced changes in R_2 of a cat brain, the changes in cerebral blood volume *in vivo* have also been quantified, suggesting the strong possibility of noninvasive quantification of physiological changes in the perfused tissues induced by any hemodynamic stimuli.

In general, tissue oxygen level is the resultant of the oxygen availability (nutritive blood flow × arterial O_2 concentration) and the rate of oxygen consumption by the cells. In normal tissues the oxygen supply and its consumption are tightly coupled to meet the requirements of the cells under changing physiologic condi-

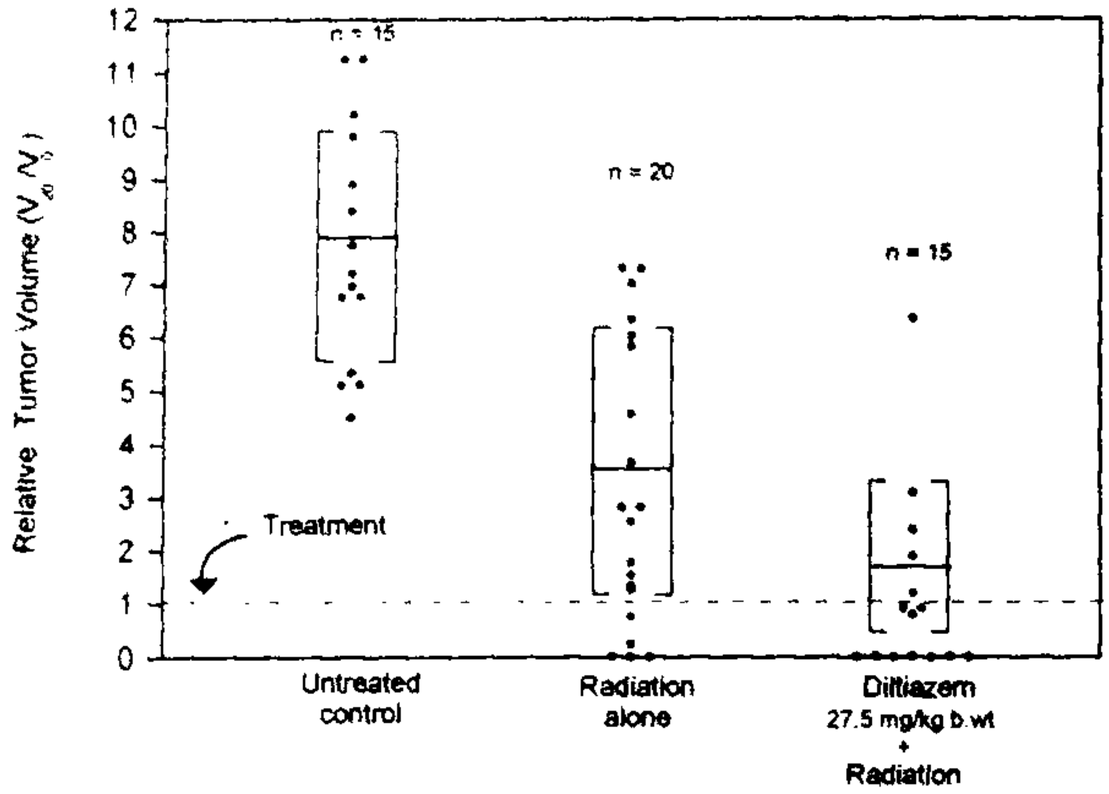

Figure 4. Diltiazem-induced enhancement in the radiation response of mice EAT. Diltiazem (27.5 mg/kg) was administered 30 *min prior* to focal ^{60}Co-γ irradiation (10 Gy, single fraction). The tumour volume at the time of treatment (V_0) was 0.8–1.0 cm^3 in all groups. The relative tumour volume analyses, after 20 day post-irradiation time (V_{20}/V_0), show considerable tumour regression in diltiazem + radiation group. The parallel bars (with dividers) in each group show the relative mean tumour volume and the corresponding standard deviation.

tions. This is accomplished by modulating tissue blood flow and/or changing the O_2 utilization (metabolic uptake of O_2) in accordance with alteration in physiological conditions. In poorly perfused tumours, however, modulations of both mechanisms are rather limited.

By using Fick's conservation law, the oxygen delivery and the oxygen uptake in tissues, in the steady state, can be described as:

$$(\text{Metabolic uptake of } O_2)_{\text{tissue}} = (\text{Blood flow}_{\text{tissue}}) \times ([O_2]_{\text{arteries}} - [O_2]_{\text{veins}}). \quad (6)$$

Eq. (6) can be restated to relate deoxyhemoglobin production proportionally to metabolic uptake and blood flow:

$$\text{dHb} \propto (\text{Metabolic uptake of } O_2)_{\text{tissue}} / (\text{Blood flow})_{\text{tissue}}. \quad (7)$$

As has been discussed earlier, the mechanism of MR-BOLD-contrast development in tissues during any hemodynamic perturbations is based on the changes in blood susceptibility ($\Delta\chi$) as a function of the tissue oxygenation (i.e. dHb levels in tissue blood pool)[58,59]. The MR signal attenuation due to the BOLD effect is well described[80] as

$$\Delta R_2^* = f(\Delta b_v . \Delta\chi), \quad (8)$$

where the susceptibility change,

$$\Delta\chi = f(\text{dHb}),$$

and Δb_v is the change in fractional blood volume (blood present in the vascular compartments of the tissue).

The fractional blood volume change, Δb_v depends on (i) the vascular morphology and architecture such as vessel size, macrovessels vs capillary composition, vessel orientation; and (ii) the functional nature of the vasculature-like increase in the population of active vessels or dilation of the vessels against a physiologic stimulus[80]. Thus the factor Δb_v mainly reflects the tissue physiologic status. The second factor, the susceptibilty change ($\Delta\chi$) which depends on the deoxyhemoglobin (dHb) levels, as stated earlier, is in turn governed by the blood supply and metabolic uptake of O_2 in tissues. For example, in a model calculation[29], where the blood vessel network is assumed to be a system containing randomly distributed cylinders with random orientation, the changes in BOLD signal can be expressed by the relation

$$\Delta R_2^* = 4/3 . \Pi . \gamma . \Delta\chi . B_0 . [((1-Y) . \Delta b_v) - b_v . \Delta Y], \quad (9)$$

where γ is the gyromagnetic ratio of the protons, B_0 is the strength of the applied external magnetic field, b_v is the fractional blood volume and ΔY is the change in the oxygenation level Y of the blood. In cerebral physiology, the relationship between the blood flow and blood volume has been reported[83] to be $(b_v)_a/(b_v)_0 = (F_a/F_0)^{0..5}$, where F_0, $(b_v)_0$ and F_a, $(b_v)_a$ are the blood flow and blood volumes before and after hemodynamic perturbation, respectively. Since the values of b_v can be obtained indirectly from the quantitative blood flow estimations using exogenous contrast enhanced MRI, therefore, in principle, it is possible to quantitate the changes in oxygen levels of the blood.

In the context of tumours, development of appropriate BOLD-contrast models, based on the present knowledge of the nature of tumour vasculature and hemodynamics, could help to derive quantitative tumour oxygenation maps from BOLD-MR measurements. Such an endeavour would immensely help in the diagnostic as well as the prognostic evaluation of tumours. Thus, the future work on the use of MRI in experimental oncology should be directed towards achieving this goal.

Conclusion

The possibility to monitor the changes in tumour blood flow and oxygenation, noninvasively, by dynamic MRI provides a potential way to probe the intricacies in tumour physiology and heterogeneity. The inter- and intratumoural heterogeneity in tumour blood flow and oxygenation can be well observed by using exogenous paramagnetic contrast agents such as Gd-DTPA and BOLD

contrast enhanced MRI respectively. Complementary use of both these techniques would help in evaluating the efficacy of tumour blood flow/oxygenation modifying agents and the responses of tumours to treatments. Finally, this approach could be useful in optimizing the therapeutic protocols of individual patients and thereby improving the treatment outcome.

1. Jain, V. K., Porschen, W. and Feinendegen, L. E., *Indian J. Exp. Biol.*, 1977, **15**, 714–718.
2. Jain, V. K., Kalia, V. K., Sharma, R., Mahajan, V. and Menon, M., *Int. J. Radiat. Oncol. Biol. Phys.*, 1985, **11**, 943–950.
3. Brown, J. M., *Cancer Res.*, 1998, **58**, 1408–1416.
4. Vaupel, P., Kallinowski, F. and Okunieff, P., *Cancer Res.*, 1989, **49**, 6449–6465.
5. Dvorak, H. F., Nagy, J. A. and Dvorak, A. M., *Cancer Cell*, 1991, **3**, 77–85.
6. Warren, B. A., in *Tumour Blood Circulation* (ed. Peterson, H. I.), CRC Press, Boca Raton, 1979, pp. 1–47.
7. Jain, R. K. *Cancer Res.*, 1988, **48**, 2641–2658.
8. Vaupel, P., *Radiat. Res. Proc. Wurzberg*, 1996, **1**, 773–778.
9. Bhaumik, K. and Jain, V., *J. Biol. Phys.*, 1991, **18**, 45–56.
10. Jirtle, R. L, *Int. J. Hyperthermia*, 1988, **4**, 355–371.
11. Horsman, M. R., Chaplin, D. J. and Overgaard, J., *Radiother. Oncol.*, 1991, **20**, 47–52.
12. Fisher, M. and Grotta, J., *Drugs*, 1993, **46**, 961–975.
13. Song, C. W., Makepeace, C. M., Griffin, R. J., Hasegawa, T., Osborn, J. L., Choi, I. and Nah, B. S., *Int. J. Radiat. Oncol., Biol. Phys.*, 1994, **29**, 433–437.
14. Lyung, H., Skretting, A. and Rofstad, E. K., *Cancer Res.*, 1992, **52**, 584–592.
15. Reinhold, H. S. and Visser, J. W. M., *Int. J. Microcirc. Clin. Exp.*, 1983, **2**, 143–146.
16. Zenke, K., Nakagawa, K., Kumon, Y., Ohta, S., Hatakeyama, T. and Sakaki, S., *J. Neuro. Oncol.*, 1996, **30**, 26–36.
17. Song, C. W., Chelstrom, L. M. and Levitt, S. H., *Int. J. Radiat. Oncol., Biol. Phys.*, 1989, **17**, 1041–1047.
18. Simpson, S. E. and Evelhoch, J. L. (Abstr) *Proc. Soc. Magn. Reson. Med.*, 1997, **1**, 492.
19. Mattiello, J. and Evelhoch, J. L., *Magn. Reson. Med.*, 1991, **18**, 320.
20. Hunjan, S., Mason, R. P., Constantinescu, A., Peschke, P., Hahn, E. W, Antich, P. P., *Int. J. Radiat. Oncol., Biol. Phys.*, 1998, **41**, 161–171.
21. Thomas, C., Counsell, C., Wood, P. and Adams, G. E., *J. Natl. Cancer Inst.*, 1992, **84**, 174–180.
22. Al-Hallaq, H. A, River, J. N., Zamora, M., Oikawa, H. and Karczmar, G. S., *Int. J. Radiat. Oncol., Biol. Phys.*, 1998, **41**, 151–159.
23. Robinson, S. P, Howe, F. A., Rodrigues, L. M., Stubbs, M. and Griffiths, J. R., *Semin. Radiat. Oncol.*, 1998, **8**, 197–207.
24. Griebel, J., Mayr, N. A., de Vries, A., Knopp, M. V., Gneiting, T., Kremser, C., Essig, M., Hawighorst, H., Lukas, P. H. and Yuh, W. T. C., *J. Magn. Reson. Imaging*, 1997, **7**, 111–119.
25. Rosen, B. R., Belliveau, J. W., Vevea, J. M. and Brady, T. J., *Magn. Reson. Med.*, 1990, **31**, 9–21.
26. Donahue, K. M., Burstein, D., Manning, W. J. and Gray, M. L., *Magn. Reson. Med.*, 1994, **32**, 66–76.
27. Kennan, R. P., Zhong, J. and Gore, J. C., *Magn. Reson. Med.*, 1994, **31**, 9–21.
28. Fisel, C. R., Ackerman, J. L., Buxton, R. B., Garrdo, L., Belliveau, J. W., Rosen, B. R. and Brady, T. J., *Magn. Reson. Med.*, 1991, **17**, 336–347.
29. Yablonsky, D. A. and Haacke, E. M., *Magn. Reson. Med.*, 1994, **32**, 749–763.
30. Weisskoff, R. M., Hoppel, B. J. and Rosen, B. R., (Abstr) *J. Magn. Reson. Imaging*, 1992, **2**, 77.
31. Donahue, K. M., Weisskoff, R. M. and Burstein, D., *J. Magn. Reson. Imaging*, 1997, **7**, 102–110.
32. Nagele, T., Petersen, D., Klose, U., Grodd, W., Optiz, H., Gut, E., Martos, J. and Voigt, K., *Am. J. Neuroradiol.*, 1993, **14**, 89–98.
33. Fuiji, K., Fujita, N., Hirabuki, N., Hashimoto, T., Miura, T. and Kozuka, T., *Am. J. Neuroradiol.*, 1992, **13**, 1215–1220.
34. Maeda, M., Itoh, S., Kimura, H., Iwasaki, T., Hayashi, N., Yamamoto, K., Ishii, Y. and Kuboto T., *Radiology*, 1993, **189**, 133–283.
35. Mayr, N. A., Yu, W. T. C., Mangotta, V. A., Ehrhardt, J. C., Wheeler, J. A., Sorosky, J. I., Davis, C. S., Chen Wen, B., Martin, D. D., Pelsang, R. E., Buller, R. E., Oberley, L. W., Mellenberg, D. E. and Hussey, D. H., *Int. J. Radiat. Oncol., Biol. Phys.*, 1996, **36**, 623–633.
36. Hittmair, K., Gomiscek, G., Langenberger, K., Recht, M., Imhof, H. and Kramer, J., *Magn. Reson. Imaging*, 1994, **31**, 567–571.
37. Crosby, D. L., Simonson, T. M., Fisher, D., Mangotta, V. A., Sato, Y. and Rezal, K., (Abstr) *Radiology*, 1994, **193** (suppl), 460.
38. Brix, G., Rempp, K., Guckel, F., Hoffman, U., Semmler, W. and Lorenz, W. J., *Adv. MRI Contrast*, 1994, **2**, 68–77.
39. Lauffer, R. B., *Chem. Rev.*, 1987, **87**, 901–927.
40. Sorensen, A. G., Tievsky, A. L., Ostergaard, L., Weisskoff, R. M. and Rosen, B. R., *J. Magn. Reson. Imaging*, 1997, **7**, 47–55.
41. Hoppel, B. E., Weisskoff, R. M., Thulborn, K. R., Moore, J. B., Kwong, K. K. and Rosen, B. R., *Magn. Reson. Med.*, 1993, **30**, 715–723.
42. Hawighorst, H., Kopp, M. V., Debus, J., Hoffman, U., Grandy, M., Griebel, J., Zuna, I., Essig, M., Schoenberg, S. O., De Vries, A., Brix, G. and van Kaick, G., *J. Magn. Reson. Imaging*, 1998, **8**, 783–788.
43. De Vries, A., Judmaier, W. and Griebel. J., (Abstr). *Int. J. Radiat. Oncol., Biol. Phys.* 1996, 36 (suppl), 377.
44. Wang, Z., Su, M. Y., Najafi, X. and Nalcioglu, O., (Abstr) *Proc. Soc. Magn. Reson. Med.*, 1997, **2**, 1089.
45. Su, M. Y., Wang, Z., Roth, G. M., Lao, X. and Nalcioglu. O., (Abstr) *Proc. Soc. Magn. Reson. Med.*, 1997, **2**, 1090.
46. Muruganandham, M., Kasiviswanathan, A., Jagannathan, N. R., Jain, P. C. and Jain, V., (Abstr) *Indian J. Nucl. Med.*, 1997, **12**, 161.
47. Henning, J., Nauesth, A. and Friedburg, H., *Magn. Reson. Med.*, 1986, **3**, 823–833.
48. Schenck, J. F., *Ann. N. Y. Acad. Sci.*, 1992, **649**, 285–301.
49. Pauling, L. and Coryell, C. D., *Proc. Natl. Acad. Sci. USA*, 1936, **22**, 210–216.
50. Thulborn, K. R., Waterton, J. C., Mathews, P. M. and Radda, G. K., *Biochem. Biophys. Acta*, 1982, **714**, 265–270.
51. Brooks, R. A. and Chiro, G. D., *Med. Phys.*, 1987, **14**, 903–913.
52. Gomori, J. M., Grossman, R. J., Yu-Ip, C., and Asakura, T., *J. Comput. Assist. Tomogr.*, 1987, **11**, 684–690.
53. Matwiyoff, N. A., Gasporovic, C., Mazurchuk, R. and Matwiyoff, G., *Magn. Reson. Imaging*, 1990, **8**, 295–301.
54. Hayman, L. A., Ford, J. J., Taber, K. H., Saleem, A, Round, M. E. and Bryan, R. N., *Magn. Reson. Imaging*, 1988, **168**, 489–491.
55. Wright, G. A., Hu, B. S. and Macovski, A., *J. Magn. Reson. Imaging*, 1991, **1**, 275–283.
56. Weisskoff, R. M., Kiihne, S., *Mag. Reson. Med.*, 1992, **24**, 375–383.
57. Schenck, J. F., *Med. Phys.*, 1996, **23**, 815–850.
58. Ogawa, S, Lee, T. M., Nayak, A. S., Glynn, P., *Magn. Reson. Med.*, 1990, **14**, 68–78.

59. Ogawa, S., Tank, D. W., Menon, R., Ellerman, J. M., Kim, S. G., Merkle, H. and Ugurbil, K., *Proc. Natl. Acad. Sci. USA*, 1992, **89**, 5951–5955.
60. Kwong, K. K., Belliveau, J. W., Chesler, D. A., Goldberg, I. E., Weisskoff, R. M., Poncelet, B. P., Kennedy, D. N., Hoppel, B. E., Cohen, M. S., Turner, R., Cheng, H. M., Brady, T. J. and Rosen, B. R., *Proc. Natl. Acad. Sci. USA*, 1992, **89**, 5675–5679.
61. Bandettini, P. A., Wong, E. C., Hinks, R. S., Tikofsky, R. S. and Hyde, J. S., *Magn. Reson. Med.*, 1992, **25**, 390–397.
62. Turner, R., Jezzard, P., Wen, H., Kwong, K. K., Le Bihan, D., Zeffiro, T. and Balaban, R. S., *Magn. Reson. Med.*, 1993, **29**, 277–279.
63. Atalay, M. K., Forder, J. R., Chacko, V. P., Kawamoto, S. and Zerhouni, E. A., *Radiology*, 1993, **189**, 759–764.
64. Karczmar, G. S., River, J. N., Li, J., Vijayakumar, S., Goldman, Z. and Lewis, M. Z., *NMR Biomed.*, 1994, **7**, 3–11.
65. Pellar, L., Weissfloch, L., Stehling, M., Weber, J., Bruening, R., Senekowitsch-Schmidtke, R., Molls, M. and Reiser, M., *Magn. Reson. Imaging*, 1998, **16**, 799–809.
66. Pellar, M., Weissfloch, L., Weber, J., Senekowitsch-Schmidtke, R., Molls, M. and Reiser M., (Abstr.) *Proc. Soc. Magn. Reson. Med.*, 1998, **1**, 58.
67. Howe, F. A., Robinson, S. P. and Grifiths, J. R., (Abstr.). *Proc. Soc. Magn. Reson. Med.*, 1993, **1**, 642.
68. Robinson, S. P., Howe, F. A. and Griffiths, J. R., *Int. J. Radiat. Oncol. Biol. Phys.*, 1995, **33**, 855–859.
69. Dunn, J. F., Zaim, Wadghiri, Y., Meyerand, M. E., O'Hara, J. A., Hickey, W. and Hoopes, P. J., (Abstr.) *Proc. Soc. Magn. Reson. Med.*, 1997, **2**, 1091.
70. Robinson, S. P., Rodrigues, L. M., Ojugo, A. S. E., Mcsheehy, P. M., Howe, F. A. and Griffiths, J. R., *Br. J. Cancer*, 1997, **75**, 1000–1006.
71. Griffiths, J. R., Taylor, N. J., Howe, F. A., Saunders, M. I., Robinson, S. P., Hoskin, P. J., Powell, M. E., Thoumine, M., Caine, L. A. and Baddeley, H., *Int. J. Radiat. Oncol. Biol. Phys.*, 1997, **39**, 697–701.
72. Howe, F. A., Robinson, S. P. and Griffiths, J. R., *NMR Biomed.*, 1996, 208–216.
73. Robinson, S. P., Howe, F. A. and Griffiths, J. R., (Abstr) *Proc. Soc. Magn. Reson. Med.*, 1997, **2**, 1092.
74. Muruganandham, M., Kasi Viswanathan, A., Jagannathan, N. R., Raghunathan, P., Jain, P. C. and Jain, V., (Abstr) *Proc. Soc. Magn. Reson. Med.*, 1998, **2**, 842.
75. Hasse, A., Frahm, J., Matthaei, D., Hanicke, W. and Merboldt, K. D., *J. Magn. Reson.*, 1986, **67**, 258.
76. Muruganandham, M., Kasi Viswanathan, A., Jagannathan, N. R., Raghunathan, P., Jain, P. C. and Jain, V., *Int. J. Radiat. Oncol., Biol. Phys.*, 1999, **43**, 413–421.
77. Ogawa, S., Menon, R. S., Tank, D. W., Kim, S. G., Merckle, H., Ellerman, J. M. and Ugurbil, K., *Biophys. J.*, 1993, **64**, 803–812.
78. Weisskoff, R. M., Zuo, C. S., Boxerman, J. L. and Rosen, B. R., *Magn. Reson. Med.*, 1994, **31**, 601–610.
79. Boxerman, J. L., Bandettini, P. A., Kwong, K. K., Baker, J. R., Davis, T. L., Rosen, B. R. and Weisskoff, R. M., *Magn. Reson. Med.*, 1995, **34**, 4–10.
80. Boxerman, J. L., Hamberg, L. M., Rosen, B. R. and Weisskoff, R. M., *Magn. Reson. Med.*, 1995, **34**, 555–566.
81. Bandettini, P. A. and Wong, E. C., *Int. J. Imaging Syst. Technol.*, 1995, **6**, 133–152.
82. van Zijl, P. C. M., Eleff, S. M., Ulatowski, J. A., Oja, J. M. E., Ulug, A. M., Traystman, R. J. and Kauppinen, R. A., *Nat. Med.*, 1998, **4**, 159–167.
83. Grubb, R. L., Raichle, M. E., Eichling, J. O. and Ter Pogossian, M. M., *Stroke*, 1974, **5**, 630–639.

ACKNOWLEDGEMENTS. This work was carried out as part of the project INM-280. The facilities at the Department of NMR, AIIMS, New Delhi, were used for MRI experiments.